

Mass and energy capture from stellar winds for magnetized and unmagnetized planets: implications for atmospheric erosion and habitability

Eric G. Blackman^{1,2,3*}, John A. Tarduno^{1,3†}

¹*Department of Physics and Astronomy, University of Rochester, Rochester NY, 14627, USA*

²*Laboratory for Laser Energetics, University of Rochester, Rochester NY, 14623, USA*

³*Department of Earth and Environmental Sciences, University of Rochester, Rochester NY, 14627, USA*

ABSTRACT

The extent to which a magnetosphere protects its planetary atmosphere from stellar wind ablation depends upon how well it prevents plasma from entering and how well it traps otherwise escaping plasma. We focus on the entering, and provide a simple formalism for estimating upper limits on mass and energy capture, the latter of which determines maximum mass loss rates. Our approach quantifies a competition between two effects: a sufficiently strong planetary magnetic field deflects incoming plasma, but also increases the mass loading cross section when the wind and planetary fields are oriented for magnetic reconnection. The rate of mass loading can be larger for a magnetized versus an unmagnetized planet even if the rate of energy loading is correspondingly less. We find this to be the case for Earth’s history since the lunar forming impact– the likely start of the geodynamo. However, polar focusing can increase the local energy flux beyond that without a magnetosphere for a strong enough planetary field and weak enough wind, and we find that this may be the case for Earth’s future. The future protective role of Earth’s magnetic field would then depend on its ability to trap outgoing plasma. Generally, the competition between increased collection area and reduced inflow speed from a magnetosphere is likely essential in determining the net protective role of planetary fields and its importance in sustaining habitability. The competing effects may also help explain why current ion loss rates from Mars, Venus and Earth are similar.

Key words: planets and satellites: magnetic fields; planets and satellites: terrestrial planets; X-rays: stars; stars: winds, outflows Earth; stars: activity

1 INTRODUCTION

Traditionally, planetary habitable zones are defined as the range of distances from a star within which a planet can orbit such that stellar luminosity heats the planet to a temperature range that can sustain gravitationally bound liquid water (Huang 1960; Kasting, Whitmire & Reynolds 1993). However, even if liquid water is essential, the potentially catastrophic effect of stellar activity from ultraviolet and X-ray photons, and stellar winds on the planetary atmosphere must also be considered (e.g. Lammer 2013). High energy photons can photo-dissociate molecules and/or heat atoms such that that the atmospheric constituents exceed the escape speed at the exobase and are catastrophically

lost. Complementarily, a strong stellar wind can exchange momentum with the planetary atmosphere and directly or indirectly eject the essential constituents.

The overall effects of stellar activity on atmospheres are commonly (if not misleadingly) delineated as ”thermal” or ”non-thermal” mechanisms (e.g. Seager 2010; Lammer 2013). For the former, energy is primarily absorbed and converted to thermal energy that for which the potential for ejection amounts to a comparison between thermal velocities and escape speed. Non-thermal mechanisms refer to a change of chemistry or ionization state of the influenced particles. Erosion of atmospheres by stellar winds is an important example of the latter, and the focus of the present paper. Ultimately, a realistic determination of habitability will depend on understanding the high energy coronal activity from stars and the efficacy with which planetary atmo-

* E-mail: blackman@pas.rochester.edu

† E-mail: john.tarduno@rochester.edu

spheres are protected against the associated radiation and winds.

Stellar activity is magnetic activity and magnetic field strength, X-ray activity, and rotation rate have long been known to correlate with each other (Noyes et al. 1984; Schrijver & Zwaan 2000; Pizzolato et al. 2003; Mamajek & Hillenbrand 2008; Wright et al. 2011; Vidotto et al. 2014). They generally increase for younger, faster rotating solar-like stars, although the x-ray luminosity flattens with rotation rate flattens for very fast rotators (Wright et al. 2011; Reiners, Schüssler & Passegger 2014). Connections between stellar activity, rotation, and magnetic field strength are all connected to the dynamo origin of these fields within the stars and is an ongoing enterprise of research to understand these connections and make them quantitative Karak, Kitchatinov & Choudhuri (2014); Kitchatinov & Olemskoy (2015); Sood, Kim & Hollerbach (2016); Blackman & Owen (2016). In the absence of significant cooling, the winds from solar-like stars, which also draw from the coronal magnetic and thermal energy are also likely significantly stronger for younger stars. This too however, is debated and a topic of active research (Wood 2006; Wood et al. 2014; Cohen 2011; Suzuki et al. 2013; Matt et al. 2015; Blackman & Owen 2016).

Planetary magnetospheres are widely perceived to be protection against erosion from stellar winds. This is of topical interest in understanding the evolution of the early Earth (Tarduno et al. 2015) and well as the potential habitability of exoplanets (do Nascimento et al. 2016) The planetary magnetic field acts as a magnetic cage that tempers stripping by stellar winds by redirecting the flow, at a bow shock, around and behind the planet. The bow shock lies just outside the radius of the "obstacle" namely the magnetopause, where the ram pressure of the stellar wind is balanced by the magnetospheric pressure of the planetary atmosphere. For example, the difference between the current water inventory of Earth versus that of Mars has long been thought to be due to the presence of an internally generated magnetic field on the former (e.g. Luhmann, Johnson & Zhang 1992; Lundin, Lammer & Ribas 2007).

However, some observations have also led to speculation that the magnetosphere might not be exclusively protective (Brain et al. 2013). For example, the present-day total atmospheric ion escape from Earth, Mars and Venus appears to be within similar orders of magnitude, at 10^{24} - 10^{26} ions s^{-1} (Barabash 2010; Strangeway et al. 2010; Wei et al. 2012). Because Earth has an internal geomagnetic field and Mars and Venus do not, the role of the internal magnetic field might seem to be un-influential. Note that understanding the present kinematic loss rates and the role of the magnetic field does not by itself determine relative habitability. The latter also depends on the long term history of each planetary atmosphere that includes its chemistry and in particular, water loss (Tarduno, Blackman & Mamajek 2014), which is crucial for life.

The competing influences of planetary magnetic fields are also manifest in their role of channeling ions. Incoming ions are channeled toward the poles in a large scale dipole configuration. In this respect, magnetic fields might exacerbate atmospheric loss rather than abate it (Brain et al. 2013). Such an effect would preferentially eject heavy ions that would otherwise be gravitational bound at atmospheric

temperatures, unlike light ions like H^+ whose thermal speed would already exceed the escape speed. Supporting evidence comes from observations (Strangeway et al. 2005) that show an enhanced outward oxygen ion flux from auroral zones consistent with a 2 order of magnitude concentration of solar wind energy (Moore & Khazanov 2010). On the other hand, the dipole magnetic fields can also recapture at least some of this outgoing flux. For example, the polar outflow of O^+ from Earth today is some 9 times greater than the net loss, considering recapture in the magnetosphere (Seki et al. 2001). A local outflow might therefore not always result in a catastrophic global outflow. Moreover, the depth to which ions can be accelerated by conversion of solar wind flux into the accelerating Poynting flux also depends on competing forces such as a magnetic mirror force (Cowley & Lewis 1990).

Despite the complexities that determine the actual fate and influence of the incoming particle flux, one thing is for certain: the momentum and energy flux eroded from the atmosphere from stellar wind cannot exceed the maximum of the energy and momentum flux captured from the stellar wind. This in turn, implies an upper limit on the mass loss, if the energy or momentum conversion into escaping particles were maximally efficient. This limit does not depend on the details that could drop the actual erosion below this limit. It is both instructive and important even to constrain how an internally produced magnetic field affects this upper limit compared to a planet without an internal magnetic field. As we will see, even this comparison provides valuable conceptual and quantitative insight.

In section 2 we estimate the wind mass and energy loading rates entering the planetary atmosphere in the presence or absence of magnetic fields. We take into account magnetic reconnection when the stellar wind field is anti-aligned with the planetary field and quantify the competing effects of reduced inflow speed and increased collection area. We also include the effects of polar focusing. In section 3, we use the results of section 2 to derive upper limits on the mass loss rates for magnetized vs. unmagnetized planets. In section 4 we apply the results to Earth-like planets. Using time-evolution models for the host stellar wind ram pressure to calculate the time-dependent magnetospheric stand-off distance, we show how the mass capture rates of Earth's history generally larger than for an unmagnetized Earth over time, even though total energy capture rates, and thus maximum mass outflow rates are lower. We discuss how this conclusion changes for Earth's future when polar focusing is included. We also apply the formalism to address the mutually similar O^+ loss rates of Mars, Venus and Earth. We conclude in section 5.

2 MASS AND ENERGY LOADING WITH AND WITHOUT MAGNETOSPHERE

2.1 Standoff distance

The location of the planetary magnetopause is determined by the standoff distance from the planet r_s , where the magnetic pressure of the planet equals that of the impinging stellar wind. If the planetary magnetic field is a dipole and the stellar wind is dominated by its ram pressure, the stand-off distance r_s is then simply given by

$$\frac{r_s^3}{r_p^3} = \left(\frac{B_p^2}{8\pi\rho_w v_w^2} \right)^{1/2}, \quad (1)$$

where r_p is the radius of the planet, B_p is the magnetic field strength at the planetary surface, ρ_w and v_w are the stellar wind density and speed at r_s respectively.

2.2 Incoming mass flux with and without magnetosphere

The rate of impinging stellar wind ions entering a planet's atmosphere depends on the product of the effective area onto which ions are captured and on the speed of the inflow. A large magnetosphere increases the effective area for potential capture, but reduces the inflow speed.

More specifically, we consider mass loading to occur primarily where and when the magnetic field of the stellar wind is favorable for reconnection with that of the planetary magnetosphere. Other modes of mass loading are also occurring (Gunell et al. 2012) but it is reasonable to focus on magnetic reconnection as the primary mechanism.

Paschmann, Oieroset & Phan (2013) point out that about 50% of the time reconnection is favorable at the Earth's magnetopause. After averaging over many cycle periods, one might expect that this arises primarily because the wind field reverses with the solar magnetic cycle, so that the shear angle between the wind field and magnetospheric field would be favorable to reconnection half of the time. In practice the favorability depends on a combination of shear angle, current sheet thickness, and variation in the plasma β (ratio of plasma to magnetic pressure) across the magnetopause. Reconnection is still possible with small shear angles (and thus strong guide field) but requires more symmetry in β across the magnetopause interface than the large shear angle cases. Nevertheless, if reconnection occurs only $\sim 1/2$ the time, it is reasonable to take the average speed at which ions flow to be $\sim 1/2$ the inflow reconnection speed. During the reconnection phase, the effective collecting area of stellar wind ions can become of order the magnetopause cross section (on the dayside). Determining the overall efficacy of the magnetosphere at keeping incident wind particles out, requires accounting for the competing effects of the increased collection area with the reduced speed.

The mass per unit time collected by a planet without a magnetosphere \dot{M}_c from a stellar wind whose velocity exceeds the escape speed of the planet at its surface can be written as:

$$\dot{M}_c \simeq \frac{\pi r_p^2}{4\pi R^2} \dot{M}_w, \quad (2)$$

where \dot{M}_w is the wind mass loss rate per unit time, r_p is the planet radius, and R is the planet-star distance. In the presence of a magnetosphere, the mass collected per unit time $\dot{M}_{c,m}$ is given by

$$\dot{M}_{c,m} = \frac{\pi r_s^2}{4\pi R^2} \frac{v_{in}}{v_w} \dot{M}_w \simeq \frac{\pi r_s^2}{4\pi R^2} \frac{v_{rec}/2}{v_w} \dot{M}_w * \frac{3}{4}, \quad (3)$$

where v_{in} is the effective inflow speed; $v_{rec} = 2.67v_{in}$ is the reconnection speed; r_s is the magnetosphere radius and the latter factor of $3/4$ comes if we assume that only $\sim 1/2$ of the reconnected flow is carried on outflow closed field lines, and a fraction $\sim 1/2$ of that flow will also be returned back

the closed fields lines due to reconnection at the magnetotail. This gives $1/2 + 1/2 * 1/2 = 3/4$.

The ratio of the mass per unit time captured by a planet with a magnetosphere to that captured by the same planet without a magnetosphere is given by the ratio of Eq. (3) to Eq. (2). This is

$$Q \equiv \frac{\dot{M}_{c,m}}{\dot{M}_c} = \frac{3}{8} \left(\frac{r_s}{r_p} \right)^2 \left(\frac{v_{rec}}{v_w} \right) \quad (4)$$

Not all of the variables in Eq. (4) are independent but we can simplify crudely as follows. Reconnection at the standoff point is generally asymmetric across the current sheet and the incoming reconnection speed from wind-side toward the current is given by (Cassak & Shay 2007)

$$v_{rec} \sim 2\tilde{\chi} \left(\frac{B_w B_2^3}{4\pi(B_w + B_2)(B_w \rho_2 + B_2 \rho_w)} \right)^{1/2}, \quad (5)$$

where B_w is field on the wind-side of the magnetopause and B_2 is the planet field at the magnetosphere side of the reconnection region, and χ measures the ratio of current sheet thickness to length. For Earth at least, data suggest $B_2 > B_w$ and $B_2 \rho_w > B_1 \rho_2$ (Sonnerup et al. 2016) so v_{rec} reduces to

$$v_{rec} \sim \frac{2B_w^{1/2} B_2^{1/2}}{(4\pi\rho_w)^{1/2}} \tilde{\chi} \simeq \chi \left(\frac{B_p}{\sqrt{4\pi\rho_w}} \right) \left(\frac{r_p}{r_s} \right)^3, \quad (6)$$

where $\chi = 2\tilde{\chi}\sqrt{B_w/B_2}$, and we use the dipole scaling $B_2 = B_p(r_p/r_s)^3$ where B_p is the surface field strength. There is hidden microphysics in observations and simulations are roughly consistent with $\tilde{\chi} = 0.1$ (Cassak & Shay 2007) and in turn $0.5 \geq \chi \geq 0.1$ for magnetopause applications, with the lower end for Earth and higher end for Venus (used later). Combining Eqs. (6) and (1) with Eq. (4) we obtain

$$v_{rec}/v_w = (8/3)v_{in}/v_w = \chi\sqrt{2}, \quad (7)$$

and thus

$$Q = 5.25 \left(\frac{\chi}{0.1} \right) \left(\frac{r_s/r_p}{10} \right)^2, \quad (8)$$

where we have scaled to present day Earth-like values of χ and r_s/r_p . That Q can exceed unity for reasonable parameters highlights the important effect of the increased collecting area that the magnetosphere provides. Eq. (8) shows that the weaker the wind, the higher the rate of mass capture for a magnetized planet relative to unmagnetized planet since r_s/r_p increases for weaker stellar winds.

2.3 Focusing toward the polar caps

Magnetic polar caps subtend a solid angle no larger than that of a hemisphere (2π) and could be much less as in the case of Earth. When captured particles are loaded toward the polar caps due to the magnetic field instead of being uniformly distributed over a hemisphere, the associated local mass flux (mass per unit time per area) and energy flux within the cap solid angle would be enhanced by a factor $1/f_c$, where

$$f_c = (1 - \cos\theta_c) \leq 1 \quad (9)$$

is the areal fraction of a hemisphere subtended by a polar cap of colatitude θ_c .

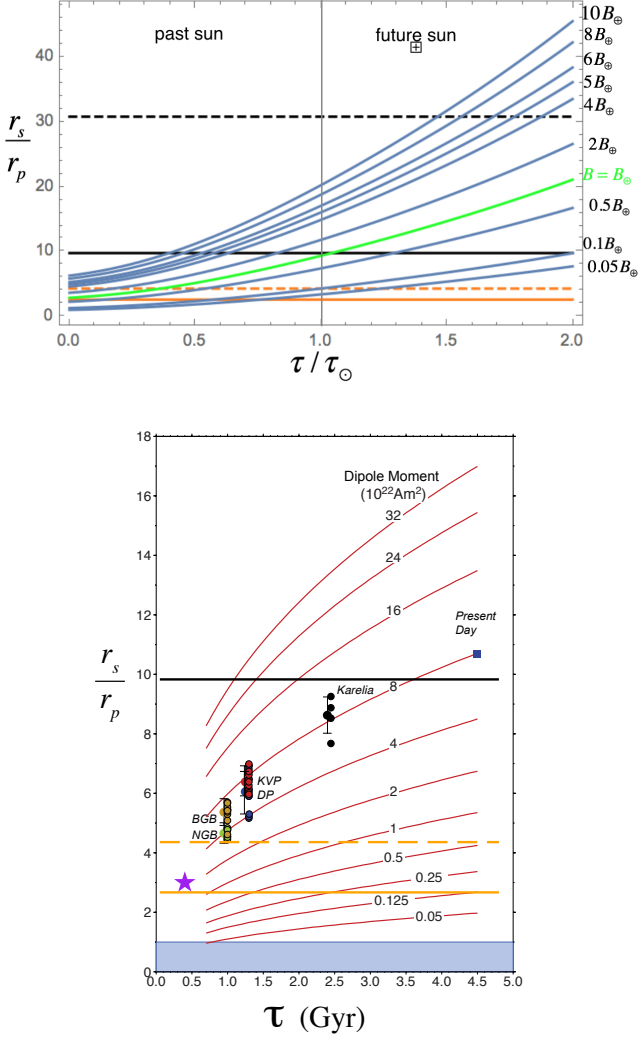


Figure 1. Standoff distance in units of Earth-like planet radius vs. age for different planet dipole moments and different wind evolution models: top (Blackman & Owen 2016); bottom figure adapted from (Tarduno et al. 2010). Green in top panel corresponds to line with its endpoint at present day measurements. Polar wind model curves in bottom panel result from combining mass loss X-ray flux correlation with X-ray flux age correlation (see text). Magnetic dipole data sources for bottom panel are as follows: Karelia (Smirnov, Tarduno & Pisakin 2003), KVP, DP (Kaaopvaal Pluton, Dalmien Pluton respectively) (Tarduno et al. 2007), and BGB, NGB (Barberton Greenstone Belt, Nondweni Greenstone Belt) (Tarduno et al. 2010). Purple star represents minimum standoff implied by paleomagnetic data from Hadean (> 4 Ga) zircons (Tarduno et al. 2015) and a solar wind model adapted from Suzuki (Suzuki et al. 2013). The geodynamo may have started shortly after the lunar forming event, when core chemical stratification was disrupted (e.g. Jacobson et al. 2017). In both panels: solid orange and black lines are thresholds of r_s/r_p above which mass (Eq (15) and energy and (18) , respectively, per solid angle toward the poles are higher for a magnetized planet. Dashed orange is the threshold above which a magnetized planet captures more total wind mass than without (Eq. 8) . Dashed black is the analogous threshold for energy (Eq (17) , and correspondingly, the threshold above which magnetized planet could incur more mass loss and (22) than an unmagnetized planet. (Dashed black is absent on bottom panel due to the smaller ordinate range.)

For present purposes, we consider only the case when the incoming wind flow is perpendicular to the planet’s magnetic dipole axis. We can then estimate θ_c for a dipole from the argument that the equation for the local polar geometry of field lines satisfies (Russell, Luhmann & Strangeway 2016)

$$r \frac{d\theta}{dr} = \frac{B_\theta}{B_r}. \quad (10)$$

For a vector dipole field in spherical coordinates of magnetic moment \mathbf{m}

$$\mathbf{B}(\mathbf{r}) = \frac{|\mathbf{m}|}{|\mathbf{r}|^3} (2 \cos \theta \hat{\mathbf{r}} + \sin \theta \hat{\theta}), \quad (11)$$

from which the ratio of the two field components is

$$\frac{B_\theta}{B_r} = \frac{\tan \theta}{2}. \quad (12)$$

Using Eq. (12) in Eq. (10) and integrating gives

$$r = r_e \sin^2 \theta, \quad (13)$$

where r_e is the value of r at which a particular field line crosses the equator ($\theta = \pi/2$). The value $\theta = \theta_c$ is determined by setting $r_e = r_s$, the magnetopause radius, and $r = r_p$ because the field lines anchored on the two polar circles $\theta = \theta_c$ at $r = r_p$ represent the anchor loci of the closed field lines just at the inner edge of the magnetopause. Field lines anchored with $\theta \leq \theta_c$ extend into the wind-side of the magnetopause, along which wind plasma can only enter during reconnection. Using the aforementioned substitutions in Eq. (13) along with Eq. (9) gives

$$f_c = 1 - \sqrt{1 - r_p/r_s}. \quad (14)$$

We see that f_c decreases with decreasing magnetic field for a fixed wind mass flux, since this would increase r_p/r_s . Correspondingly, for a fixed planetary magnetic field, f_c decreases with increasing wind ram pressure. This implies that f_c would generally increase with stellar age for steady planetary field strengths.

We define $q \equiv Q/f_c$ as the ratio of mass capture rate per solid angle by a magnetized planet that includes polar cap channeling to that in the absence of a magnetosphere altogether. From Eq. (8) we then obtain

$$q \simeq \frac{Q}{f_c} \simeq 52.5 \left(\frac{\chi}{0.1} \right) \left(\frac{r_s}{10r_p} \right)^3 \left[1 + \left(1 - \frac{r_p}{r_s} \right)^{1/2} \right], \quad (15)$$

where the factor in square brackets varies only between 1 and 2. Note that $q/Q = 1/f_c$ increases with stellar youth.

Taken at face value, Eqs. (8) and Eqs. (15) highlight that the mass flux captured by a magnetized Earth-like planet, when averaged over many field reversal periods, could be greater than without a magnetic field. Our analysis here supersedes that in Tarduno, Blackman & Mamajek (2014) where we did not give an explicit expression for the reconnection speed, quantify polar focusing, emphasize that Q and q can exceed unity while the analogous energy rate ratio can still be much less than unity. We discuss the latter below, as it is most important in assessing mass loss.

2.4 Incoming energy flux with and without magnetosphere

The ratio of energy input rates imparted to the atmosphere for magnetized vs. unmagnetized planets can be obtained by multiplying Eq. (8) and Eq. (15) by

$$\xi = \frac{\left(\frac{c_s^2}{\Gamma-1} + v_{in}^2\right)}{\left(\frac{c_s^2}{\Gamma-1} + v_w^2\right)} = \frac{\left(\frac{c_s^2/v_w^2}{\Gamma-1} + 0.28\chi^2\right)}{\left(\frac{c_s^2/v_w^2}{\Gamma-1} + 1\right)}, \quad (16)$$

where c_s is the incoming sound speed and Γ is the adiabatic index. This internal energy term for the incoming material of sound speed c_s is added to the inflow energy to account for the total energy flux. Multiplying Eq. (8) and Eq. (15) by Eq. (16) then gives the ratios of energy capture rates of the magnetized to unmagnetized planet for unfocused and polar focused cases as

$$Q_{en} \sim 0.11 \left(\frac{\xi}{0.02}\right) \left(\frac{\chi}{0.1}\right) \left(\frac{r_s/r_p}{10}\right)^2 \quad (17)$$

and

$$q_{en} = \frac{Q_{en}}{f_c} \simeq 1.1 \left(\frac{\xi}{0.02}\right) \left(\frac{\chi}{0.1}\right) \left(\frac{r_s}{10r_p}\right)^3 \left[1 + \left(1 - \frac{r_p}{r_s}\right)^{1/2}\right], \quad (18)$$

respectively. The scaling value of $\xi = 0.03$ arises if we use fiducial values for the incoming wind of $c_s \simeq 3.9 \times 10^6$ cm/s (corresponding to $T \simeq 10^5$ K), $v_w = 400$ km/s, and $\Gamma = 5/3$. Eq. (17) shows that the total energy collected by an magnetized planet scaled to present day Earth-sun-like parameters is comfortably less than that of the magnetized planet. However Eq. (18) shows that the polar energy flux concentration can be comparable, or even greater for the magnetized planet.

3 CONNECTING LOADING TO LOSS: UPPER LIMITS ON MASS LOSS RATE

The exact determination of the induced mass loss from an incoming stellar wind depends upon detailed plasma and chemical properties that determine how the incoming energy gets converted to outgoing particles (Sibeck et al. 1999; Lammer 2013; Russell, Luhmann & Strangeway 2016). The extent to which the field can trap the outgoing particles can also limit the otherwise induced energetic particle loss. But regardless of how the energy and momentum inputs are subsequently converted into outgoing particles, we can estimate and compare the maximum mass loss rates that the wind could cause, for magnetized and unmagnetized cases. The distinction between these two cases is essential when the exobase is below the magnetopause or ionopause.

The maximum atmospheric mass loss can be determined from use of conservation of momentum and energy with the actual maximum being determined by which of these two conservation estimates gives the larger value. Specifically, the upper limit on mass loss corresponds to the circumstance in which all of the incoming momentum or energy is transferred to outgoing particles moving just at the escape speed associated with the exobase. The wind energy flux times the capture area for inflow speed v_{in} is given by

$$\rho_{in} A v_{in} \left(\frac{c_s^2}{\Gamma-1} + v_{in}^2\right) = \dot{M}_{in} \left(\frac{c_s^2}{\Gamma-1} + v_{in}^2\right), \quad (19)$$

and the wind momentum flux times the capture area is

$$\rho_{in} A \left(v_{in}^2 + \frac{c_s^2}{\Gamma}\right) = \dot{M}_{in} v_{in} \left(1 + \frac{c_s^2}{\Gamma v_{in}^2}\right). \quad (20)$$

The maximum outflow mass loss rate is estimated simply by assuming the maximally efficient case in which all of the incoming momentum or energy gets converted into outflow with all outflowing particles moving exactly at the escape speed v_{esc} estimated at the exobase. If the ratio of the inflow speed to the escape speed exceeds unity, then energy conservation determines the upper limit. Otherwise momentum conservation determines the limit. For a steady state, the corresponding energy and momentum rate balance equations for inflow and outflow are given respectively by

$$\dot{M}_{in} \left(\frac{c_s^2}{\Gamma-1} + v_{in}^2\right) = \dot{M}_{out} v_{esc}^2, \quad (21)$$

and

$$\dot{M}_{in} v_{in} \left(1 + \frac{c_s^2}{\Gamma v_{in}^2}\right) = \dot{M}_{out} v_{esc}. \quad (22)$$

By rearranging each of Eq. (21) and (22) to obtain an expression for \dot{M}_{out} , we can combine the results to express the maximum of the two upper limit estimates for the outflow mass loss. If we also allow for the polar focusing fraction f_c , the combined result is

$$\frac{\dot{M}_{out,max}}{M_{in}} = \frac{1}{f_c} \frac{v_{in}}{v_{esc}} \text{Max} \left[\frac{v_{in}}{v_{esc}} \left(1 + \frac{c_s^2/v_{in}^2}{\Gamma-1}\right), \left(1 + \frac{c_s^2/v_{in}^2}{\Gamma}\right) \right], \quad (23)$$

where the first term in brackets is the result from energy conservation and the second term is from momentum conservation. The former dominates when $v_{in} > v_{esc}$, and the latter when $v_{in} < v_{esc}$. Note that if all the energy and momentum instead went into particles moving at some speed $v_{ave} > v_{esc}$ then v_{ave} would replace v_{esc} in Eq. (23) and the mass outflow rate estimate would be correspondingly reduced.

4 IMPLICATIONS FOR ATMOSPHERE PROTECTION

Having built up the formalism in the previous two sections, we now discuss the direct application of these results to the time evolution of magnetospheric protection for the Earth-sun system and to the separate question of present day Oxygen ion loss rates from Earth, Mars, and Venus.

4.1 Influence of stellar activity variation on the protective role of the magnetosphere

The blue curves of the top panel and the red curves of the bottom panel of Fig. 1 show the time evolution of r_s/r_p for different values of the planetary magnetic field (assumed to be constant for each curve) for an Earth-like planet at 1AU from a sun-like star. The top panel uses the minimalist, but holistic theoretical model of (Blackman & Owen 2016) to compute the standoff distance from the wind ram pressure. The latter is derived from the time evolution of magnetic

field, rotation, mass loss, and X-ray luminosity predicted from the physics of the model. Although the correlation between X-ray luminosity and stellar mass loss has been questioned (Cohen 2011), this query is based on short-term observations of the Sun that may not apply to the billion year time scales of interest. The bottom panel in Fig. 1 shows curves from Tarduno et al. (2010) which utilize the empirical mass loss values for solar-like stars from (Wood 2006) based on H I Lyman- α data. Those values are observed to correlate with X-ray flux, which in turn was used to empirically determine stellar ages. The magnetopause standoff distances are truncated at 700my because the few available young stellar analogs hint at lower rates of mass loss (Wood et al. 2014), breaking the correlation. (The saturation of X-ray flux with youth also makes age determination more difficult for younger stars (Mamajek & Hillenbrand 2008; Wright et al. 2011).) An alternative theoretical model, which focuses on Alfvén wave driving and includes cooling (Suzuki et al. 2013), can be used to obtain solar wind ram pressure estimates for these young solar ages (see Tarduno, Blackman & Mamajek (2014)).

The green curve in the top panel of Fig. 1 corresponds to that which matches the present day field measurements, as also labeled on the bottom panel. The curves of both panels show that r_s/r_p decreases with youth because of the stronger ram pressure of the solar wind, while the planetary field remains nearly constant. The horizontal lines in the two panels of Fig 1 correspond to the specific thresholds calculated in Section 2. Namely, the orange solid lines show the threshold of r_s/r_p above which $q \geq 1$ from Eq. (15) (assuming the lower limit of 1 for the square bracketed quantity). The orange dashed lines show the threshold above which $Q \geq 1$ from Eq. (8). These are respectively the thresholds above which the polar and total mass collection rates for the magnetized planet exceed those for the unmagnetized planet. Analogously, the solid and dashed black curves, which correspond to Eqs (18) (assuming the lower limit of 1 for the square bracketed quantity) and (17) respectively, indicate the threshold ratio of r_s/r_p above which the polar focused, and total energy capture rates by the magnetized planet exceed that for an unmagnetized planet. Because energy conservation (rather than momentum conservation) determines the the extremum in Eq. (23) for Earth-sun-like systems, these curves also indicate the corresponding thresholds above which the magnetized planet has higher upper limits on mass loss from stellar-wind atmosphere erosion than the unmagnetized planet.

Given the fiducial parameter values used to make the horizontal lines, both panels of Fig. 1 have the same qualitative implications: for most of an Earth-like planet’s history, more total mass and polar mass flux can be captured by a magnetized planet than for a correspondingly unmagnetized planet even though less total energy is captured by the magnetized planet over its past history. As shown for the choice of fiducial parameters of the Earth-sun system, this circumstance will also persist for the the long term future. In turn, since the maximum mass outflow rate for an Earth-sun-like system is determined by energy rather than momentum in Eqn. (23), use of the total energy without polar focusing (i.e. setting $f_c = 1$) would in turn imply that the upper limit on the mass loss rate would be reduced by a magnetosphere throughout the Earth-like planet’s past and future.

If however, we include polar focusing using f_c from Eq. (9), the solid black horizontal lines of Fig 1 exemplify that the captured polar energy flux and associated upper limit on mass outflow rate can be *higher* in the recent past and future for the magnetized Earth compared to an unmagnetized Earth. That is, the magnetosphere could actually allow a higher maximum outflow than in the absence of a magnetic field for future Earth because of the higher incoming energy flux collected. Here the two panels differ somewhat in where the line crosses the standoff curve that best matches present day but as alluded to above, neither the data nor the models are yet accurate enough for this time scale to be pinned down to better than factor of 2.

How close the actual mass loss corresponds to these upper limits depends on the important details of how the incoming energy an momentum flux are further processed, but the conceptual point that the upper limit can be large with a magnetosphere under certain circumstances is noteworthy.

4.2 Partial explanation of why present-day O^+ loss from Mars, Venus, and Earth are similar

Oxygen ion (O^+) loss in Earth, Mars and Venus must involve solar wind-ion interaction, to gain enough energy for to reach the escape speed (Dubinin et al. 2011; Wei et al. 2012). In practice, photoionization and dissociative recombination convert neutral molecules into O^+ which can become pickup ions trapped by the solar wind magnetic field, and carried away by the solar wind inertia. But as mentioned in the introduction, the issue of why O^+ ion loss rates on Earth, Mars and Venus are so similar, given their different magnetospheric properties, has led some to question the exclusively protective role of an internally generated magnetosphere (Strangeway et al. 2010; Wei et al. 2012).

While the detailed processes and local conditions within the different atmospheres are different, and measured rates themselves depend on solar activity phase and spacecraft location, we can nevertheless use the our formalism to obtain upper limits to the escape rates to exemplify how competing effects can conspire in the different planet cases and account for the observed range of mass loss rates. Zendejas, Segura & Raga (2010), presented a different minimalist model of ion outflow rates, using an imposed efficiency parameter α to characterize ho much inflow energy gets converted to outflow. A value $\alpha = 1$ would make their results also upper limits. However, they do not address the magnetized case and our interest here is in comparing unmagnetized with magnetized cases. Cohen et al. (2014) and Cohen et al. (2015) provide a numerical MHD study of M-star stellar winds interacting with habitable magnetized and Venus-like planets to obtain standoff distances and lower limits on mass loss, and highlight the need to combine chemistry and microphysics to obtain detailed models. Our focus here is specifically on upper limits of mass loss which depends less on the detailed microphysics, using the simple formalism of the previous sections.

For solar system planets, use of Eq. (23) for $f_c = 1$, along with Eq. (7) and Eq. (3) gives

$$\dot{M}_{out} \leq 1.1 \times 10^5 \left(\frac{\dot{M}_w}{1.3 \times 10^{12} \text{g/s}} \right) \left(\frac{v_w}{4 \times 10^7 \text{cm/s}} \right)^2 \left(\frac{\chi}{1} \right)^3 \times \left(\frac{r_s}{r_e} \right)^2 \left(\frac{R}{\text{IAU}} \right)^{-2} \left(\frac{r_{ew}}{r_e} \right) \left(\frac{M_p}{M_e} \right)^{-1} \left(\frac{3.6c_s^2 / [\chi^2 v_w^2 (\Gamma - 1)] + 1}{1} \right) \text{g/s}, \quad (24)$$

where R is the planet-sun distance, M_p is the planet mass, r_{ex} is the exobase radius and the latter along with the stand-off distance r_s are scaled to Earth's radius r_e .

For Earth, $r_{ex} \sim 1.2r_e$ and $r_s \sim 10r_e$, $\chi = 0.1$ and the last factor in parenthesis of Eq. (24) is 5.6 so the result is $\dot{M}_{out} \leq 6.3 \times 10^4 \text{g/s}$. The associated particle loss rate limit is then

$$dn/dt \leq \frac{\dot{M}_{out,max}}{\mu m_p} \simeq 4.7 \times 10^{27} \left(\frac{\mu}{8}\right)^{-1} \text{s}^{-1}, \quad (25)$$

where This can be compared with $7.2 \times 10^{25}/\text{s}$ of O^+ observed with speeds above escape leaving the poles, and averaged over a solar cycle (Seki et al. 2001), of which 90% is actually recaptured.

For Venus there is little appreciable separation between the stand-off distance and the planet radius. Here the stand-off distance is determined by the ionopause particle pressure, although the induced magnetic field just outside this is observed to have a value in near equipartition with the internal thermal pressure (Russell, Luhmann & Strangeway 2016). Penetrating the the ionosphere still requires reconnection so that v_{in} is determined by a reconnection speed, but the ionopause and exobase are only a few 100km from the surface making the effect radii r_s and r_{ex} comparable to r_e . The lower magnetic field and slightly higher solar magnetic field at Venus make ξ (defined below Eq. (6)) slightly higher for Venus. In applying Eqn. (23) we use $\chi = 0.4$; $r_s \sim r_{ex} \sim r_e$; $R = 0.72 \text{AU}$; $M_p = 0.81 M_e$, and thus 1.3 for the last factor in parenthesis to obtain $\dot{M}_{out} = 1.9 \times 10^3 \text{g/s}$. The corresponding ion loss rate is then

$$dn/dt \leq \frac{\dot{M}_{out,max}}{\mu m_p} \simeq 1.6 \times 10^{27} \left(\frac{\mu}{8}\right)^{-1} \text{s}^{-1}. \quad (26)$$

This limit is few times larger than the highest values reported (Knudsen & Miller 1992) and at least an order of magnitude larger than more typical values as summarized in Dubinin et al. (2011).

For Mars, aside from its localized magnetic features, much of the surface has too little magnetic or ionospheric pressure to match the incoming wind ram pressure. As the relevant incoming mass loading flow speed is now $v_{in} \sim v_w$ so that $0.28\chi^2 = 1$ (from Eq. (7) and the last factor in parenthesis of Eqn. (23) is ~ 1 . Combining this with use of $M_p = 0.11 M_e$; $r_p \sim r_s = r_{ex} = 0.53 r_e$, and $R = 1.5 \text{AU}$ in Eqn. (23), we obtain $\dot{M}_{out} = 6.6 \times 10^4 \text{g/s}$. The corresponding ion loss rate is then

$$dn/dt \leq \frac{\dot{M}_{out,max}}{\mu m_p} \simeq 5 \times 10^{27} \left(\frac{\mu}{8}\right)^{-1} \text{s}^{-1}. \quad (27)$$

This can be compared with values up to $1.5 \times 10^{25}/\text{s}$ at solar max reported in Dubinin et al. (2011).

While the particle loss rates estimated above are strictly upper limits, their mutual similarity is noteworthy given the very different magnetosphere environments of the three planets. This similarity results largely because of the competing effects whereby a large magnetosphere can increase collecting area for incoming wind particles but also reduce the incoming speed. For Earth, the incoming speed is reduced from the wind speed, but the collecting area is significantly increased. For Venus the incoming speed is not quite as reduced as it is for Earth, but the collecting area is substantially reduced. For Mars, the incoming speed is un-

abated and the collecting area is just the planet radius, and the planet is farthest of the three from the sun.

As mentioned earlier, turning the upper limits into actual estimates requires more detailed modeling. However, recall from the discussion below Eq. (23) that if the average escaping particle has a much higher speed than v_{esc} , then the particle loss rate estimates would decrease. It is a worthy pursuit to try and identify the basic principles that dictate how efficiently the incoming energy is redistributed among particles and on what this depends. For example, the denser the environment of interaction between the wind and the atmosphere, the more evenly the energy is likely distributed. This may help explain why actual loss rates measured for Venus are typically a bit closer to the estimated upper limits than for Earth and Mars.

In short, our formalism may help to explain the mutually similar present-day loss rates of the terrestrial planets having atmospheres. We reiterate that this is separate from the more general question of the role of magnetic fields in sustaining habitability. In particular, the probative value of present-day Venus and Mars in exploring this question is limited because their present state reflects a longterm atmospheric evolution with profound loss of the principal component defining habitability- water. For Venus, in particular, present-day atmospheric erosion rates are irrelevant because of the dearth of water, and uninhabitability of the planet.

Finally, we note that the implications of our results are consistent with those of Wei et al. (2012) who reported measurements from 4 spacecrafts comparing increases in the outflow of O^+ from Earth and Mars during an increase in solar wind dynamic pressure. They found that the outflow flux (number per unit time per area) from Mars increased by a factor of 60 whereas the outflow from Earth increased by only a factor of 7. As we have shown, the magnetosphere can reduce energy inflow and thus reduce mass outflow even if the total mass inflow is higher with a magnetosphere. Keeping this consistency between our results and those of Wei et al. (2012) in mind, note however that the latter represents a comparison of how local outflow responds to changes in incoming wind ram pressure, not how a unmagnetized vs. magnetized planet responds to fixed combination of stellar wind and magnetosphere circumstances; a magnetized planet with a large magnetosphere could collect more mass than an unmagnetized planet even if the magnetized planet better protects locally against changes in incoming wind flux.

5 CONCLUSIONS

We have considered how a planetary magnetosphere influences the upper limit on stellar wind induced mass loss by focusing on the how the magnetic field affects the incoming flow of mass and energy into the atmosphere. The maximum outflow rates are estimated by converting all of the incoming energy to outgoing particles just at the escape speed. Our formalism can be used to obtain rough upper limit estimates for a given planetary magnetic field, planet size, mass, orbital radius and stellar wind parameters. The basic formalism may be helpful toward a better understanding of the role magnetic fields play in protecting atmospheres of both solar system and extrasolar planets.

Converting the upper limits to actual direct estimates

of mass ejection depend on the details of energy and momentum conversion beyond the present scope. But the upper limits are nevertheless valuable, both conceptually and quantitatively. In particular, Earth's history close to the present date appears to be dominated by the case where more mass but less energy has been collected than were the magnetic field absent and unsustainable by the geodynamo.

However, our formalism also highlights that incoming incoming mass and polar energy fluxes can, under certain circumstances actually be larger with a magnetic field than without. This implies that without considering the role of the magnetic field in trapping otherwise ejected outgoing particles, the planetary magnetic field is not always guaranteed to be protective. In particular, this may be the case for the future Earth. We showed how the competing effects of reduced inflow speed and large collecting area can conspire in the Earth-sun system to cause more total mass to be collected with the field than without. And when polar focusing is taken into account, the future polar energy flux collected by Earth's magnetosphere can exceed that which would be collected without a field. The latter implies that the future protective effect of the geomagnetic field depends on its ability to recapture (Seki et al. 2001) otherwise ablated plasma.

We also showed that the same competing effects might contribute to explaining the mutually similar O^+ ion ejection rates from Earth, Mars, and Venus.

Further work on this topic can include more detailed time evolution models of stellar winds, more general orientation of the planetary magnetic field to the incoming wind direction, and incorporation of the present results into models that also track the actual fate of solar wind pickup ions and the extent to which the upper limits are close to actual limits.

ACKNOWLEDGMENTS

We thank J. Carroll-Nellenback and J. E. Owen for useful related discussions. EB acknowledges support from grants NSF-AST-1109285 and HST-AR-13916.002 and from the Simons Foundation, the Institute for Advanced Study (Princeton) and the Kavli Institute for Theoretical Physics of UCSB with support from NSF grant PHY-1125915. JAT acknowledges support from grants NSF-EAR-1656348 and NSF-EAR-1520681.

REFERENCES

- Barabash S., 2010, in EGU General Assembly Conference Abstracts, Vol. 12, EGU General Assembly Conference Abstracts, p. 5308
- Blackman E. G., Owen J. E., 2016, *MNRAS*, 458, 1548
- Brain D., Leblanc F., Luhmann J., Moore T., Tian F., 2013, *Planetary Magnetic Fields and Climate Evolution*, Mackwell S. J., Simon-Miller A. A., Harder J. W., Bullock M. A., eds., *Space Science Series*, Univ. of Arizona, Tucson, pp. 487–501
- Cassak P. A., Shay M. A., 2007, *Physics of Plasmas*, 14, 102114
- Cohen O., 2011, *MNRAS*, 417, 2592
- Cohen O., Drake J. J., Gloer A., Garraffo C., Poppenhaeger K., Bell J. M., Ridley A. J., Gombosi T. I., 2014, *ApJ*, 790, 57
- Cohen O., Ma Y., Drake J. J., Gloer A., Garraffo C., Bell J. M., Gombosi T. I., 2015, *ApJ*, 806, 41
- Cowley S. W. H., Lewis Z. V., 1990, *Planetary and Space Science*, 38, 1343
- do Nascimento, Jr. J.-D. et al., 2016, *ApJL*, 820, L15
- Dubin E., Fraenz M., Fedorov A., Lundin R., Edberg N., Duru F., Vaisberg O., 2011, *Space Science Reviews*, 162, 173
- Gunell H. et al., 2012, *Physics of Plasmas*, 19, 072906
- Huang S.-S., 1960, *PASP*, 72, 106
- Jacobson S. A., Rubie D. C., Hernlund J., Morbidelli A., Nakajima M., 2017, *Earth and Planetary Science Letters*, 474, 375
- Karak B. B., Kitchatinov L. L., Choudhuri A. R., 2014, *ApJL*, 791, 59
- Kasting J. F., Whitmire D. P., Reynolds R. T., 1993, *Icarus*, 101, 108
- Kitchatinov L. L., Olemskoy S. V., 2015, *Research in Astronomy and Astrophysics*, 15, 1801
- Knudsen W. C., Miller K. L., 1992, *JGR*, 97, 17
- Lammer H., 2013, *Origin and Evolution of Planetary Atmospheres*
- Lammer H., Lichtenegger H. I. M., Khodachenko M. L., Kulikov Y. N., Griessmeier J., 2011, in *Astronomical Society of the Pacific Conference Series*, Vol. 450, *Molecules in the Atmospheres of Extrasolar Planets*, Beaulieu J. P., Dieters S., Tinetti G., eds., p. 139
- Luhmann J. G., Johnson R. E., Zhang M. H. G., 1992, *Geophys. Res. Lett.*, 19, 2151
- Lundin R., Lammer H., Ribas I., 2007, *Space Science Reviews*, 129, 245
- Mamajek E. E., Hillenbrand L. A., 2008, *ApJ*, 687, 1264
- Matt S. P., Brun A. S., Baraffe I., Bouvier J., Chabrier G., 2015, *ApJL*, 799, L23
- Moore T. E., Khazanov G. V., 2010, *J. Geophys. Res.*, 115, A00J13
- Noyes R. W., Hartmann L. W., Baliunas S. L., Duncan D. K., Vaughan A. H., 1984, *ApJ*, 279, 763
- Paschmann G., Oieroset M., Phan T., 2013, *Space Science Reviews*, 178, 385
- Pizzolato N., Maggio A., Micela G., Sciortino S., Ventura P., 2003, *A&A*, 397, 147
- Reiners A., Schüssler M., Passegger V. M., 2014, *ApJ*, 794, 144
- Russell C., Luhmann J., Strangeway R., 2016, *Space Physics: An Introduction*. Cambridge University Press
- Schrijver C. J., Zwaan C., 2000, *Solar and Stellar Magnetic Activity*. Cambridge Univ. Press
- Seager S., 2010, *Exoplanet Atmospheres: Physical Processes*
- Seki K., Elphic R. C., Hirahara M., Terasawa T., Mukai T., 2001, *Science*, 291, 1939
- Sibeck D. G. et al., 1999, *Sp. Sci. Rev.*, 88, 207
- Smirnov A. V., Tarduno J. A., Pisakin B. N., 2003, *Geology*, 31, 415
- Sonnerup B., Paschmann G., Haaland S., Phan T., Eriksson S., 2016, *Journal of Geophysical Research (Space Physics)*, 121, 3310
- Sood A., Kim E.-j., Hollerbach R., 2016, *ApJL*, 832, 97

- Strangeway R., Russell C., Luhman J., Moore T., Foster J., Barabash S., Nilsson H., 2010, in 2010 Fall Meeting, AGU Abstracts, Vol. 129, EGU General Assembly Conference Abstracts, pp. SM33B–1893
- Strangeway R. J., Ergun R. E., Su Y.-J., Carlson C. W., Elphic R. C., 2005, *J. Geophys. Res.*, 110, A03221
- Suzuki T. K., Imada S., Kataoka R., Kato Y., Matsumoto T., Miyahara H., Tsuneta S., 2013, *Publ. Astron. Soc. Japan*, 65, 98
- Tarduno J. A., Blackman E. G., Mamajek E. E., 2014, *Physics of the Earth and Planetary Interiors*, 233, 68
- Tarduno J. A., Cottrell R. D., Davis W. J., Nimmo F., Bono R. K., 2015, *Science*, 349, 521
- Tarduno J. A., Cottrell R. D., Watkeys M. K., Bauch D., 2007, *Nature*, 446, 657
- Tarduno J. A. et al., 2010, *Science*, 327, 1238
- Vidotto A. A. et al., 2014, *MNRAS*, 441, 2361
- Wei Y. et al., 2012, *Journal of Geophysical Research-Space Physics*, 117, A03208
- Wood B. E., 2006, *Space Science Reviews*, 126, 3
- Wood B. E., Müller H.-R., Redfield S., Edelman E., 2014, *ApJL*, 781, L33
- Wright N. J., Drake J. J., Mamajek E. E., Henry G. W., 2011, *ApJ*, 743, 48
- Zendejas J., Segura A., Raga A. C., 2010, *Icarus*, 210, 539